BBA - Molecular and Cell Biology of Lipids 1870 (2025) 159687

Contents lists available at ScienceDirect

BBA - Molecular and Cell Biology of Lipids

journal homepage: www.elsevier.com/locate/bbalip

Regular paper

Age-related changes in cardiolipin profile and functional consequences of altered fatty acid supply

Philipp W. Weiß [a,b], Philip P. Kaltenborn [a,b], Christiane Frahm [c], Ulrike Schulze-Späte [d], Estelle Heyne [e], Marten Szibor [e,f,h], Sandor Nietzsche [g], Ralf A. Claus [a,b], Markus H. Gräler [a,b,h,*]

[a] Department of Anesthesiology and Intensive Care Medicine, Jena University Hospital, Am Klinikum 1, 07747, Jena, Germany
[b] Center for Molecular Biomedicine, Jena University Hospital, Hans-Knöll-Str. 2, 07745, Jena, Germany
[c] Department of Neurology, Jena University Hospital, Am Klinikum 1, 07747, Jena, Germany
[d] Section of Geriodontics, Department of Conservative Dentistry and Periodontology, Center of Dental Medicine, University Hospital Jena, Jena, Germany
[e] Department of Cardiothoracic Surgery, Jena University Hospital, Am Klinikum 1, 07747, Jena, Germany
[f] Faculty of Medicine and Health Technology, FI-33014, Tampere University, Finland
[g] Center for Electron Microscopy, Jena University Hospital, Ziegelmühlenweg 1, 07743, Jena, Germany
[h] Center for Sepsis Control and Care, Jena University Hospital, Am Klinikum 1, 07747, Jena, Germany

ARTICLE INFO

Keywords:
Phospholipid
Mass spectrometry
Aging
Mitochondria
Dietary fat
Lipid saturation

ABSTRACT

Cardiolipins (CLs) are primarily expressed in the inner mitochondrial membrane where they play essential roles in membrane architecture and mitochondrial functions. CLs have a unique structure characterized by four acyl chains with different stoichiometries such as chain length and degree of saturation. CL composition changes with disease and age, but it is largely unknown how dynamic changes affect mitochondrial function. Here, we compared CL profiles in different mouse tissues across different age groups using liquid chromatography and triple quadrupole mass spectrometry. A key finding was that CLs in the brain differ significantly from those in peripheral organs, with a tendency towards longer-chain variants. We hypothesized that these differences may be influenced by the availability of fatty acids (FA), which in the brain could be affected by the blood-brain barrier. In support of this notion, we found that FA concentrations varied in the different compartments. In addition, we found that CL profiles changed during aging. In cultivated macrophages supplemented with different FAs, we tested how altered CL profiles may affect both, mitochondrial morphology and function such as cristae density, and mitochondrial membrane potential and respiration, respectively. Finally, we validated our *in vitro* results *in vivo* by altering the CL profile in mice by using palmitic acid and oleic acid enriched diets. Our study highlights a dynamic adaptation of CL profiles in response to FA availability and aging and emphasizes its functional importance for mitochondrial function. Furthermore, FA supplementation may be a promising therapeutic strategy to address disease- and age-related mitochondrial malfunctions.

1. Introduction

Cardiolipins (CLs) are unique phospholipids found almost exclusively in the inner mitochondrial membrane (IMM) of eukaryotic cells constituting up to 20 % of the IMM's total phospholipid mass [1]. Unlike other phospholipids, CLs have a dimeric structure with two phosphate groups attached to glycerol and four acyl chains instead of two commonly found in phosphatidylcholines. This peculiar composition allows the constitution of a number of possible lipid variants. Interestingly, the stoichiometry of constituted CLs shows a great plasticity varying, for instance, with health status and age.

The unique structure of CL also leads to unusual biophysical properties with a conical shape and curvature [2]. They are critical for maintaining mitochondrial architecture including morphology and stability of mitochondrial cristae [3]. In addition, accumulating evidence indicates that CLs play a central role in regulating mitochondrial metabolic processes. For example, CLs interact with membrane-bound proteins of the respiratory chain, thus influencing electron flux

* Corresponding author at: Hans-Knöll-Str. 2, 07745, Jena, Germany.
E-mail addresses: philipp.weiss@uni-jena.de (P.W. Weiß), Christiane.Frahm@med.uni-jena.de (C. Frahm), Ulrike.Schulze-Spaete@med.uni-jena.de (U. Schulze-Späte), Estelle.Heyne@med.uni-jena.de (E. Heyne), Marten.Szibor@med.uni-jena.de (M. Szibor), Sandor.Nietzsche@med.uni-jena.de (S. Nietzsche), Ralf.Claus@med.uni-jena.de (R.A. Claus), Markus.Graeler@med.uni-jena.de (M.H. Gräler).

https://doi.org/10.1016/j.bbalip.2025.159687
Received 24 April 2025; Received in revised form 18 August 2025; Accepted 2 September 2025
Available online 7 September 2025

through the respiratory chain and indirectly the maintenance of the proton gradient across the IMM, itself the main driving force for oxidative phosphorylation (OXPHOS) [4,5]. CLs also influence signaling pathways ruling apoptosis, both, indirectly and directly as scavengers for reactive oxygen species and *via* interaction with cytochrome *c* and other pro-apoptotic factors, respectively [6,7]. Recently, CLs emerged as essential constituents of mitochondrial quality control and dynamics machineries that regulate mitochondrial fission and fusion processes [8].

Metabolism of CLs include two biological key pathways. *De novo* synthesis starts with the formation of cytidine diphosphate (CDP) diacylglycerol by consuming cytidine triphosphate [9]. This is followed by the synthesis of phosphatidylglycerol phosphate from CDP-diacylglycerol and glycerol-3-phosphate, releasing cytidine monophosphate. Then, dephosphorylation leads to the formation of phosphatidylglycerol, which subsequently condensates with another CDP-diacylglycerol to form the CL backbone [10,11]. Remodeling of CLs is a process in which the acyl residues are exchanged *via* transacylases such as tafazzin. Mutations in the tafazzin gene are known to cause Barth syndrome presenting with muscle weakness, cardiomyopathy, and neutropenia, thus giving disruption of CL metabolism clinical relevance [12–14].

Here, we set out to study how organ- and age-related changes in CL composition affect mitochondrial morphology and function and cellular/organismal viability. Indeed, organs show different FA availability and need due to blood perfusion and function. Conversely, aging is characterized by a general loss of physiological integrity, progressive functional decline, and increased mortality risk. Molecular hallmarks of aging include genetic, epigenetic, and proteomic alterations [15] progressively leading to mitochondrial dysfunction such as respiratory chain impairment [16,17]. Recent evidence indicates that also the lipidome is subject to dynamic changes in the course of life [18]. Based on these observations, we hypothesized that changes in the CL profile may underlie observed organ dysfunctions with age. To test this hypothesis, we adapted a recently established, highly sensitive liquid chromatography coupled to triple quadrupole mass spectrometry (LC-MS/MS) method under alkaline conditions to reliably detect and quantify CLs [19]. The major presence of CLs in the IMM guarantees that CLs isolated from any sample can be reliably attributed to mitochondria. With a precursor ion scan detecting a common fragment from the glycerol backbone of all CLs, we got an overview about a broad range of different CL variants. Multiple reaction monitoring (MRM) was used for exact quantification. We were able to reveal tissue- and condition-specific dependencies of CL composition with regard to the functional consequences. Also, we controlled the FA supply in supplementation experiments with cultured cells and mice to modify the CL profile actively, since the FA supply is closely related to the CL profile [20–22].

2. Methods

2.1. Mouse samples

A colony of C57BL/6J/UKJ wildtype mice was maintained in the Central Experimental Animal Facility (ZET) of the Jena University Hospital (Jena, Germany). All animals were kept under barrier conditions with a controlled 14-h light/10-h dark cycle and food and water *ad libitum* according to the ARRIVE guidelines. For aging experiments, only male mice were used, bred under above conditions and maintained at 22 ± 2°C and a relative humidity of 55 ± 10 % as described previously [23]. Palmitic acid (PA) or oleic acid (OA) enriched diets were given to 4-week-old male C57BL/6 J wildtype mice as previously described [24]. A standard diet (ND) for 16 weeks was used as control. All procedures involving animals were performed according to state and federal laws after approval by the local state authorities (UKJ-17/036 and 02–024/15).

2.2. Cell culture

The mouse macrophage cell line J774A.1 (ATCC TIB-67) was grown in DMEM – low glucose (0.9–1.1 g/L, D5546; Sigma-Aldrich, St. Louis, MA), supplemented with 10 % fetal bovine serum (FBS, 10500–064; Gibco, Invitrogen, Carlsbad, CA), 100 U/mL penicillin and 100 µg/mL streptomycin (17-602E; Lonza Group, Basel, Switzerland). The cells were cultured at 37 °C in a humidified atmosphere containing 5 % CO_2. Primary rat vascular smooth muscle cells (VSMC) were kindly provided by Bodo Levkau (University Hospital Düsseldorf, Germany) and cultured under similar conditions with high glucose (4.5 g/L) and addition of 1 mM sodium pyruvate to the culture medium.

2.3. FA supplementation in cell culture

For FA supplementation in cultured cells, we used the FAs 16:1 (Cay10009871, Biomol, Hamburg, Germany) and 18:2 (L1376, Sigma-Aldrich, St. Louis, MA). FAs were dissolved in ethanol (100 mM stock solution). The cells were grown in DMEM (low glucose) supplemented with 2 % FBS, 100 U/mL penicillin and 100 µg/mL streptomycin. FAs were added twice a day for five days to reach the target concentration of 125 µM (0.125 % maximum ethanol concentration). One medium exchange was performed on the third day.

2.4. Lipid extraction

Cells were suspended in 1 mL phosphate buffered saline (PBS). Organs were frozen in liquid nitrogen, crushed with a mortar and the powder was then dissolved in 1 mL PBS. The samples as well as 10 µL of the CL internal standards at a concentration of 500 µM (4 × 18:2d5 CL and 4 × 14:0 CL, 791108C and 750332P Avanti Polar Lipids Inc., Alabaster, AL, USA) as well as the FA internal standards in a concentration of 100 µM (17:0 d3 FA and 20:0 d3 FA, 27870, cayman, Ann Arbor, MI, USA) were pipetted into glass centrifuge tubes (Corning, Wiesbaden, Germany). 1 mL of methanol (Diagonal, Münster, Germany), 2 mL of chloroform (Carl Roth, Karlsruhe, Germany), and 300 µL of 18.5 % HCl (Carl Roth, Karlsruhe, Germany) were added. The mixture was vigorously vortexed for 10 min and centrifuged (3,000 rcf for 3 min at room temperature). After transferring the lower organic phase into a fresh glass centrifuge tube, another 2 mL of chloroform were added to the remaining methanol-saturated aqueous phase. The sample was vortexed and centrifuged a second time and the organic phases were combined in a glass vial. The solvent was evaporated under vacuum, and the extracted lipids were dissolved in 100 µL of a mixture of chloroform and methanol (50 % chloroform, 50 % methanol). The samples were analyzed by LC-MS/MS. For serum samples, we added 200 µL methanol and 10 µL each of the 100 µM FA 17:0 d3 and FA 20:0 d3 internal standards to 20 µL serum. After an overnight incubation at −80 °C, proteins were precipitated by centrifugation at 4,500 rcf and 4 °C. The supernatant was kept at −20 °C until LC-MS/MS analysis.

2.5. Identification and quantification of CLs and FAs

For CL analysis, we used a method previously described with few modifications [19]. Briefly, 10 µL sample volume was applied onto a Hamilton PRP1 2,1 × 100 mm column (CS-Chromatographie Service GmbH, Langerwehe, Germany) with 5 µm particle size using the Agilent series 1200 HPLC system (Agilent Technologies, Darmstadt, Germany). Separation of analytes was performed with 10 % solvent A (acetonitrile) and 90 % solvent B (0.5 % ammonium water) with an initial flow rate of 200 µL/min, switching to 100 % solvent A after sample injection. The flow rate increased to 400 µL/min between 5 and 7 min and switched to 10 % solvent A after 12 min and to 200 µL/min flow rate between 14 and 15 min. The program stopped after 17 min. The measurements were performed in a Sciex API 2000 triple quadrupole mass spectrometer (AB Sciex GmbH, Darmstadt, Germany) with negative electrospray

ionization (ESI). For CL identification, a precursor ion scan was performed for the fragment *m/z* 153 (glycerol 1,2 cyclic phosphate ion) with Q1 scanning between m/z 1200–1600. Quantification was performed in the MRM mode for ions carrying two negative charges with the detection of free fatty acid fragments as described [19]. The drying gas temperature of the ESI source was 450 °C and the nebulizer voltage was −4.5 kV. Curtain (CUR) and collision (CAD) gases were set to 40 psi (2.76 bar) and 2 psi (0.14 bar) respectively, and nebulizing (GS1) and drying (GS2) gases were set to 40 psi (2.76 bar) and 70 psi (4.83 bar), respectively. The declustering (DP), focusing (FP), entrance (EP), collision cell entrance (CEP) and collision cell exit potentials (CXP) of the doubly ionized CL were set at −50 V, −300 V, −4 V, −30 V and −10 V. The collision energy (CE) was set at −42 V and the dwell time at 70 ms. FAs were analyzed using an isocratic HPLC program. The mobile phase consisted of 90 % solvent A (methanol) and 10 % solvent B (0.5 % ammonium water). The program ran for 10 min at a flow rate of 400 μL/min. The declustering (DP), focusing (FP), entrance (EP), collision cell entrance (CEP) and collision cell exit potentials (CXP) were set to −40 V, −370 V, −8 V, −20 V and −10 V, respectively. The collision energy (CE) was also set at −10 V and the dwell time at 30 msec. FAs were analyzed by pseudo-fragmentation with identical values for Q1 and Q3, corresponding to the molecular weight of the respective FA ions. Standard curves were generated by adding increasing concentrations of CLs up to 300 pmol and FAs up to 100 pmol. Linearity of the standard curves and correlation coefficients were obtained by linear regression analyses ($r^2 > 0.99$). Data analyses were performed using Analyst 1.6.3 (AB Sciex GmbH, Darmstadt, Germany).

2.6. ROS assay

50,000 cells per well were incubated in 100 μL HBSS (Gibco Thermo Fisher, Waltham, MA, USA) with 10 μM 2′,7′-dichlorodihydrofluorescein diacetate (H_2DCFDA, D399, Invitrogen Thermo Fisher, Carlsbad, CA, USA) for 30 min in a 96 well plate (Greiner, Kremsmünster, Austria). The cell-permeable H_2DCFDA is a chemically reduced form of fluorescein that is used as an indicator primarily of hydroxyl radicals, peroxyl radicals, and other reactive oxygen species (ROS) in living cells. After cleavage of the acetate groups by intracellular esterases and oxidation, the non-fluorescent H_2DCFDA is converted into the highly fluorescent 2′,7′-dichlorofluorescein (DCF). The supernatant was removed and the adhered cells were resuspended with 100 μL HBSS. The measurement was performed after 90 min with a Tecan Infinite F200 plate reader (Tecan, Crailsheim, Germany) with a filter excitation of 485 nm and an emission of 535 nm.

2.7. Mitochondrial membrane potential measurement

1.0×10^6 cells were incubated in 1 mL medium with 2 μM JC-1 dye (420200, Merck, Darmstadt, Germany) for 15 min. The positive control was treated with 1 μL 50 mM of the protonophore CCCP (555–60-2, Thermo Scientific Chemicals, Carlsbad, CA, USA) for 6 min. The cells were then washed, centrifuged and resuspended in 300 μL PBS. For each measurement, 25 μL were applied to the BD Accuri C6 flow cytometer (Becton-Dickinson, Karlsruhe, Germany). The mean areas of PE and FITC signals were divided (PE-A/FITC-A). The resultant values of non-treated control cells were set to 100 %. Changes were depicted as relative values (% difference).

2.8. Transmission electron microscopy

Small pellets of cells were fixed with 2.5 % *v*/v glutaraldehyde in 0.1 M sodium cacodylate buffer (pH 7.4) for 24 h at room temperature. After washing 3 times for 15 min with 0.1 M sodium cacodylate buffer (pH 7.4), the pellets were post-fixed with 2 % *w/v* osmiumtetroxide for 1 h at room temperature. During the following dehydration in ascending ethanol series, post-staining with 1 % w/v uranylacetate was performed. Afterwards, the pellets were embedded in epoxy resin (Araldite) and sectioned using a Leica Ultracut S (Leica, Wetzlar, Germany). Finally, ultrathin sections were mounted on filmed Cu grids, post-stained with lead citrate, and studied in a transmission electron microscope (EM 900, Zeiss, Oberkochen, Germany) at 80 kV and magnifications of 3,000× to 20,000×. For image recording, a 2 K slow scan CCD camera (TRS, Moorenweis, Germany) was used. For quantitative analysis, the cristae density was determined by normalizing the total length of the cristae in a mitochondrion to its area, resulting in μm^{-1} as the unit.

2.9. Respirometry

Cellular oxygen consumption was measured at 37 °C using a Clark-type oxygen electrode (Strathkelvin, North Lanarkshire, Scotland) as previously described, with minor modifications [25,26]. Briefly, J774 control and treated (FA 16:1 and FA 18:2) cells were centrifuged for 5 min at 25 °C at 400 rcf to remove the medium and subsequently resuspended in PBS. Cells were counted using the trypan blue exclusion method and aliquoted. For respirometry, aliquots were centrifuged again for 5 min at 25 °C at 400 rcf and resuspended in respiration medium (100 mM KCl, 50 mM MOPS, 1 mM EGTA, 5 mM KH_2PO_4, and 1 mg/mL of fatty-acid-free bovine serum albumin at pH 7.4) shortly before the experiment. A total of 0.5×10^6 cells were added to 0.5 mL of respiration medium in the oxygraph chamber to first measure endogenous whole-cell respiration. Next, digitonin (20 μg; D141, Sigma-Aldrich, St. Louis, MA, USA) was added to permeabilize the cells, followed by the sequential addition of different substances (purchased from Merck, Darmstadt, Germany, and Thermo Scientific Chemicals, Carlsbad, CA) in the following order and at the indicated concentrations: pyruvate (5 mM), glutamate (5 mM), malate (2 mM), adenosine 5′-diphosphate sodium salt (ADP, 2 mM) for achieving maximal phosphorylating respiration (state 3), 2,4-dinitrophenol (0.1 mM) for achieving maximal uncoupled respiration.

2.10. Statistics

GraphPad Prism 7.0 was used for statistical significance testing. Data were tested for normal distribution using the Shapiro-Wilk test. Two groups were tested for statistical significance using the two-sample Student's *t*-test. Multiple groups were tested for statistical significance using a one-way ANOVA with Tukey's multiple comparison test. Outliers were identified using the interquartile range (IQR) method, and values exceeding 1.5 × IQR were excluded from the analysis.

3. Results

For CL quantification, we adapted a method originally described by Gang Xu and colleagues with some modifications as outlined in the methods section [19]. The calibration curves were linear over the tested concentration range of 1–300 pmol with $R^2 > 0.99$ (Fig. 1A). With the established LC separation method under alkaline conditions, we first carried out precursor ion scan measurements of lipid extracts that originated from different tissue types. For this, we used the common CL fragment of *m/z* 153, which derives from the glycerol backbone of CL. Heart and liver as well as other peripheral organs such as spleen, kidney and skeletal muscle exhibited a similar CL profile. These were characterized by a prominent peak with an *m/z* value of 1448, reflecting a CL with four 18:2-FA residues (Fig. 1B,C). Additionally, we conducted precursor ion scans to search for the specific m/z values of CLs with alternative FA composition. These scans revealed a high proportion of 18:2 FA residues in other CL variants of peripheral tissues with usually two to three 18:2 acyl chains. In contrast, brain tissue displayed a distinct profile with a higher diversity of different CL variants (Fig. 1D). We found a high proportion of 18:1-FA residues, but also high levels of longer chain polyunsaturated FAs such as 20:4-FA and 22:6-FA, resulting in CL profiles with a higher molecular weight reflected by a right

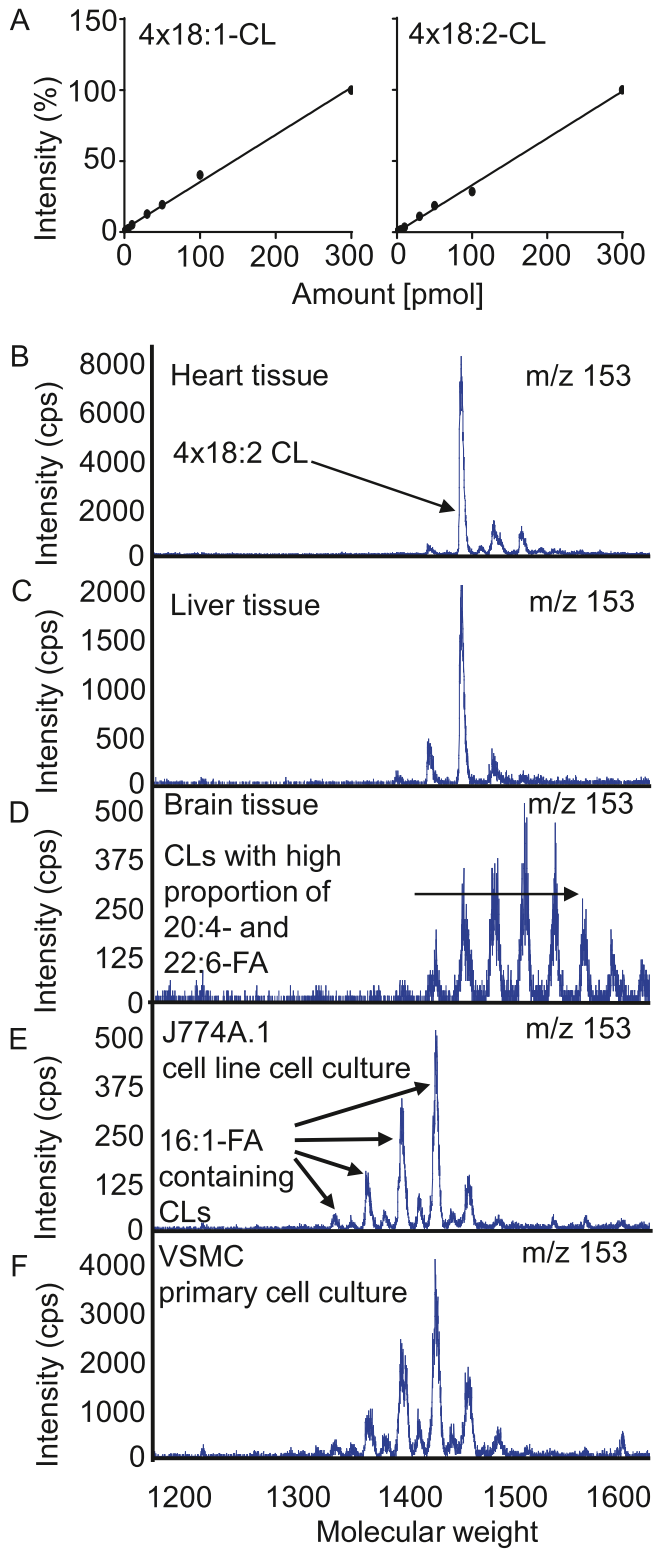

Fig. 1. (A) Standard curves for the quantification of 4 × 18:1-CL and 4 × 18:2-CL. The standards were analyzed at 1, 3, 5, 10, 30, 50, 100 and 300 pmol. Peak areas were plotted against the known amounts, fitted using linear regression and normalized to the maximal value (300 pmol = 100 %) for display. The resulting calibration curves were linear over the tested range with coefficients of determination $R^2 = 0.9956$ and $R^2 = 0.9965$. (B-F): Precursor ion scan of the fragment *m/z* 153 following lipid extraction. Representative illustration of five independent experiments of (B) mouse heart tissue, (C) mouse liver tissue, (D) mouse brain tissue, (E) cultivated J774A.1 mouse macrophages and cultivated rat vascular smooth muscle cells (VSMC, F).

shift of signals in the mass histogram. We also performed experiments with the mouse macrophage cell line J774A.1 incubated under standard conditions. A precursor ion scan of the fragment m/z 153 revealed a CL profile differing from all analyzed *ex vivo* mouse tissues with a tendency towards lower molecular masses reflecting a composition with shorter FA-chains (Fig. 1E). Indeed, LC-MS/MS measurements demonstrated a dominant proportion of 16:1-FA and 18:1-FA as side chains. Additionally, we analyzed primary cultured rat vascular smooth muscle cells (VSMCs, Fig. 1F). Surprisingly, the overall CL profile of VSMCs were similar to that observed in J774A.1 cells, indicating that cell culture conditions rather than cell specificity may determine the CL profile.

We then wanted to investigate the underlying reasons for these differences. The observed unique CL pattern in brain, separated from systemic circulation by the blood-brain barrier, prompted us to compare the supply with FAs with other peripheral tissues. Actually, the brain, generally rich in FAs, exhibited its own FA profile, which deviated significantly from that in other peripheral organs such as heart and liver. Notably, 18:2-FA, the most common FA residue in peripheral CL, reached a significantly lower concentration in the brain compared to heart or liver (Fig. 2A). Conversely, the amounts of 18:1-FA, 20:4-FA and 22:6-FA were significantly higher compared to the other tissues investigated (Fig. 2B-D). These FAs were common acyl chains in the CL of brain. Notably, our approach without prior acid hydrolysis is limited to the detection of free fatty acids only.

Specific quantification of the most abundant CLs in peripheral tissue using LC-MS/MS in MRM mode revealed that 4 × 18:2-CL, dominant in peripheral tissue, was nearly absent in the brain, which was also the case for 3 × 18:2/1 × 20:3-CL and 3 × 18:2/1 × 22:6-CL variants (Fig. 2E-G). While there were no qualitative differences between CLs of heart and liver, the concentration of individual molecular CL species tended to be lower in liver tissue. In contrast to all investigated 18:2-CL forms, the concentration of 2 × 18:1/2 × 20:4 CL was much higher in brain than in other investigated peripheral tissues, reflecting their increased presence in the brain (Fig. 2H).

Next, we examined the FA content in fetal calf serum (FBS) and compared it to adult human serum. FBS is routinely used for continuous cultivation of cells and under most experimental cell culture conditions the only source of FA. We found in FBS markedly lower levels of 18:2-FA compared to human serum (Fig. 2I). Thus, we considered the lack of 18:2-FA in FBS a critical determinant for the unique CL-profile observed in cultivated cells. The level of 18:1-FA was also significantly lower compared to human serum, but still at a much higher level than the 18:2-FA, in line with the high content of CLs with 18:1 acyl residue in cultured cells (Fig. 2J). Conversely, the concentration of the long-chain FAs 20:4-FA and 22:6-FA were much lower in human serum than in FBS (Fig. 2K, L). These observations led us to conclude that the CL-profile was strongly affected by FA availability.

To detect age-dependent changes in the CL profile, we compared samples from aged mice (29 months) with young mice (8 weeks). We focused on skeletal muscle, heart and liver tissue and determined first the proportion of 4 × 18:2-CL in the total amount for a qualitative assessment. A considerable decrease in the proportion was observed in all three tissue types with age (Fig. 3A-C). The amount of the dominant CL in the peripheral tissues thus decreased significantly with age. On the other hand, we found increased concentrations of CLs with a non-C18 acyl chain, including both shorter-chain variants with C16 acyl chains and longer-chain variants with C20 or C22 acyl chains (Fig. 3D-F). This indicates that aging is associated with a higher diversity of different CL variants across tissues.

Furthermore, we established a cell culture model that enabled the active modification of the CL profile by adding specific FAs in the same J774A.1 macrophage cell line. Previous studies using cultured cells suggested significant effects upon addition of FAs on the CL profile [27,28]. To maintain a constant FA level due to rapid cellular uptake, we added FAs twice per day for five consecutive days of incubation. Successful incorporation was confirmed by LC-MS/MS measurements using

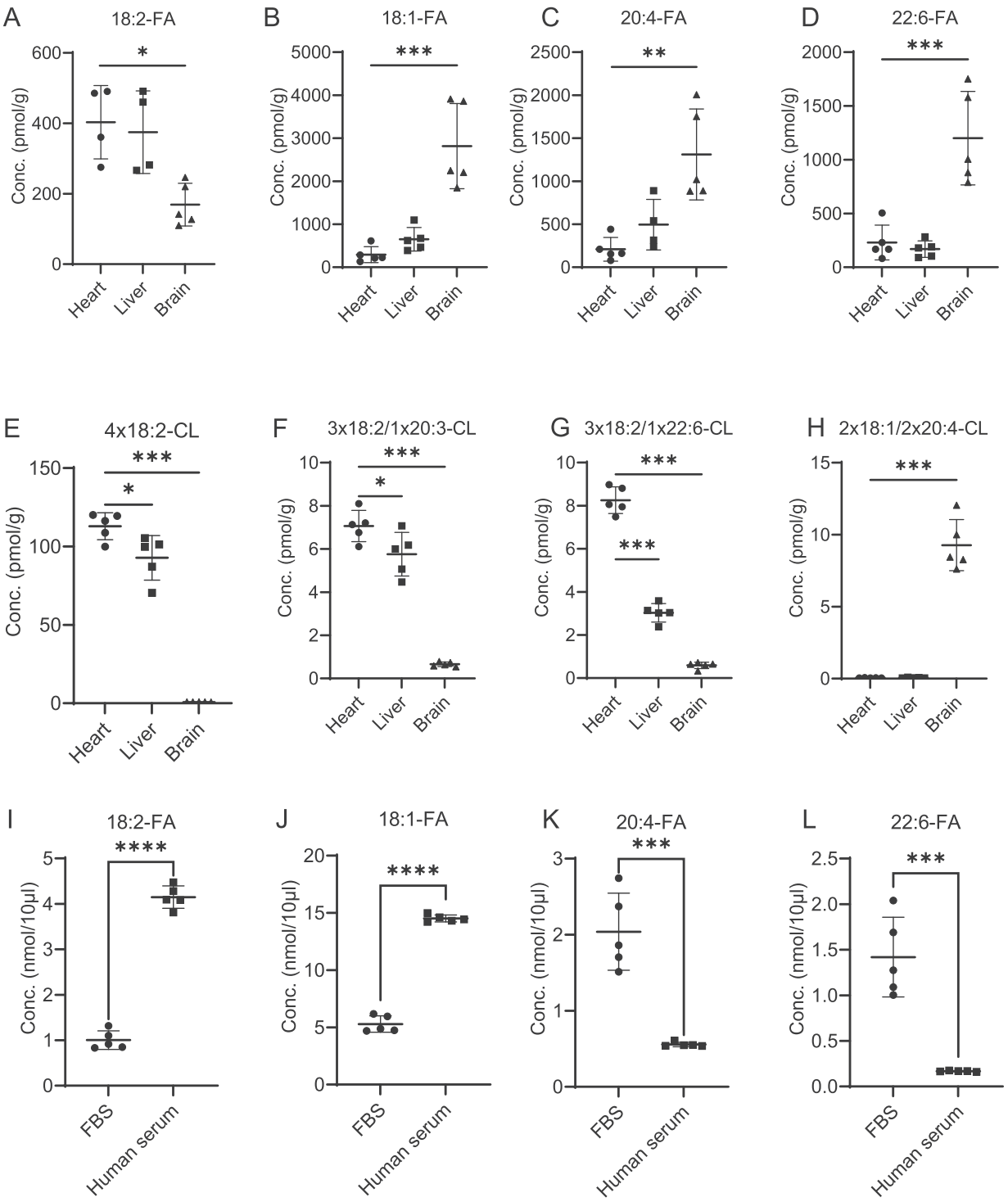

Fig. 2. Concentration of different FAs and CLs in organ systems and serum. (A-D) Comparison of 18:2-FA (A), 18:1-FA (B), 20:4-FA (C) and 22:6-FA (D) concentrations in heart, liver and brain tissue as indicated. (E-H) Comparison of the three most common CLs in the heart (E-G) and the most common CL in the brain (H). (I-L) Comparison of the concentration of FAs in fetal bovine serum (FBS) and human serum. Data are shown as mean ± SD, of 4–5 organs derived from different individual mice (A-H) or 5 different FBS and human serum samples (I-L). Statistical analysis was performed for two groups using two-sample Student's *t*-test and for multiple groups using the one-way ANOVA test followed by Tukey's multiple comparison test, with $^{*}p < 0.05$, $^{**}p < 0.01$, $^{***}p < 0.001$.

precursor ion scans of the common CL fragment *m/z* 153 (Fig. 4A). Control cells were incubated with 2 % FBS for the same period and exhibited the usual cell culture CL profile (Fig. 1D). The addition of 16:1-FA caused a shift towards lower molecular weight CLs with 16:1-FA integrated in their structure. There was also a noticeable shift towards higher molecular weight CLs after addition of 18:2-FA, indicating efficient incorporation of 18:2-FA into the CL structure. We illustrated the occurring CL shift also with quantitative measurements. The 18:2-FA substituted cells showed a constant increase of the 4 × 18:2-CL over the incubation period (Fig. 4B). After 5 days of supplementation, we measured constant high values of 4 × 18:2-CL. We then performed several functional assays to compare the mitochondrial functional state under altered CL profiles. Transmission electron microscopy imaging was conducted for morphological assessment. The control group and

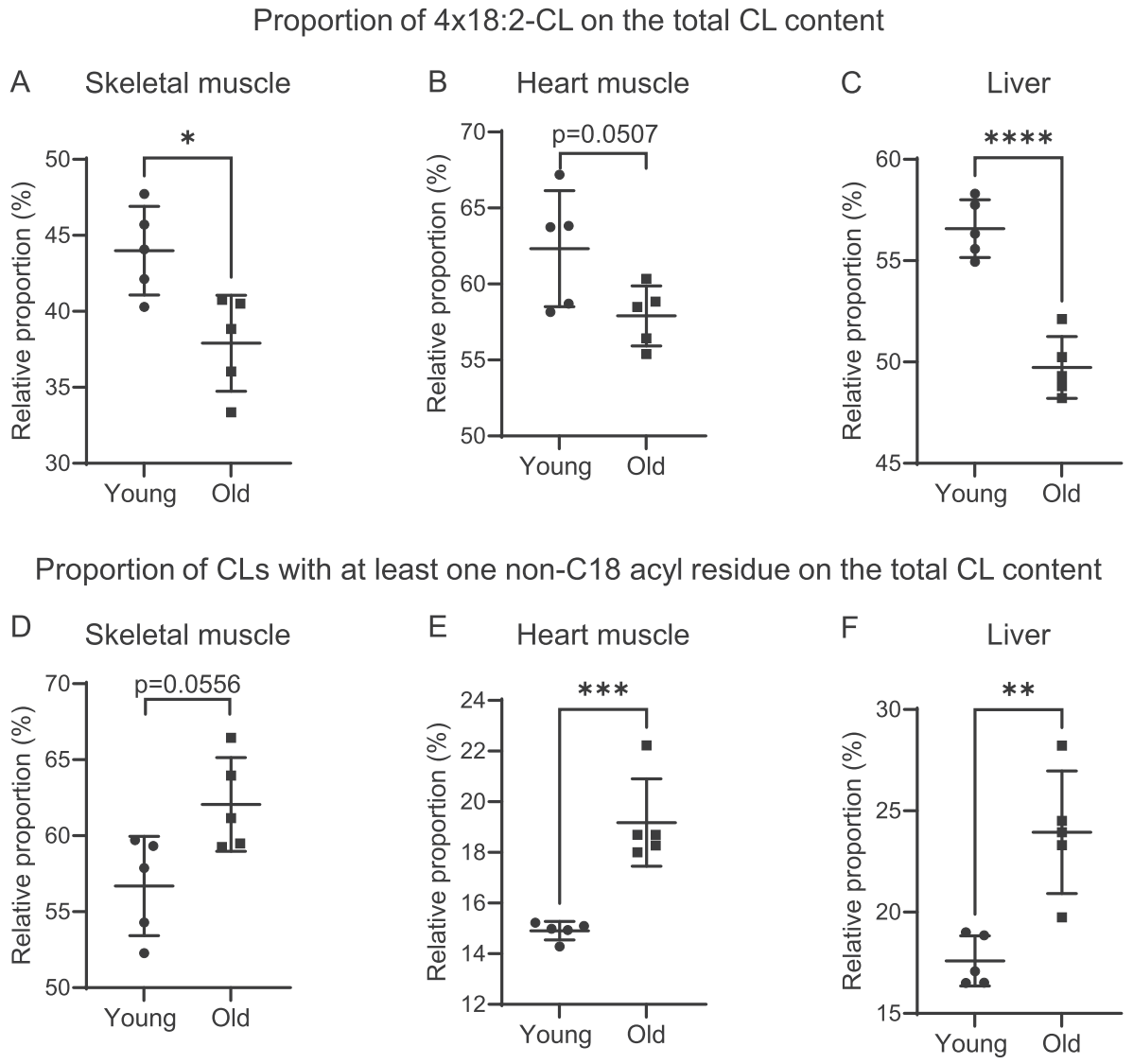

Fig. 3. Comparison of tissue samples from young mice aged 2–3 months with old mice aged 28–29 months. (A-C) Proportion of 4 × 18:2-CL on the total CL content. (D-F) Proportion of CLs with at least one non-C18 acyl residue on the total CL content. Data are shown as mean ± SD of 5 organs derived from different individual mice. Statistical analysis was performed using two-sample Student's t-test, with *$p < 0.05$, **$p < 0.01$, ***$p < 0.001$. The seven most commonly found CL-variants 4 × 18:2-CL, 3 × 18:2/1 × 18:1-CL, 3 × 18:2/1 × 16:1-CL, 2 × 18:2/1 × 18:1/1 × 16:1-CL, 3 × 18:2/1 × 20:2-CL, 3 × 18:2/1 × 20:3-CL and 3 × 18:2/1 × 22:6-CL were included in the analyses.

16:1-FA treated cells did not differ significantly, while the 18:2-FA-substituted cells had an increased cristae density (Fig. 4C). Cristae are characteristic invaginations of the inner mitochondrial membrane that increase membrane surface area, providing space for enzymatic processes [29]. A reactive oxygen species (ROS) assay revealed no significant differences in ROS levels between the experimental groups, except for the positive control treated with 10 or 100 μM H_2O_2, which exhibited increased ROS levels (Fig. 4D). A large proportion of intracellular ROS is produced as a by-product of mitochondrial activity during oxidative phosphorylation [30], but this production did not appear to be affected by the altered CL profile. We also measured mitochondrial membrane potential (MMP) using the fluorescent dye JC-1. The MMP is the product of proton pumping by a subset of respiratory chain complexes and its use as driving force for OXPHOS, thus reflecting mitochondrial activity [31]. Treatment of cells of the control group with the uncoupler carbonyl cyanide *m*-chlorophenyl hydrazine (CCCP) disrupted the membrane gradient, resulting in a lower MMP (Fig. 4E). The MMP did not differ significantly from the control group after 16:1-FA treatment, which aligns with the already high 16:1-FA content in FBS-incubated cells. In contrast, incubation with 18:2-FA led to a significant increase in MMP. Determination of the respiratory capacity (oxygen consumption) resulted in no significant differences in whole cell respiration rate in J774A.1 cells that were treated for 5 days with 125 μM 16:1-FA and 18:2-FA twice daily compared to non-treated controls (Fig. 4F). Similar results were obtained after cell permeabilization with digitonin and addition of complex I-linked substrates. However, maximal phosphorylating respiration after addition of 2 mM ADP (state 3) and uncoupled respiration after addition of 2,4-dinitrophenol were significantly reduced in both, 16:1-FA and 18:2-FA treated J774A.1 cells, indicating an impact of FA treatment on maximal and uncoupled respiration.

Finally, we set out to modulate the CL profile *in vivo* by maintaining mice on different diets, *i.e.*, 16:0-FA- or 18:1-FA-enriched diets for twelve weeks or controls on standard chow. Analysis of the FA levels in liver samples revealed a noticeable increase in the supplemented FAs compared to the control group (Fig. 5A,B). Yet, such *in vivo* supplementation of 18:1-FA in mice was shown to increase levels of pro-resolving lipid mediators and, as a consequence, increased resolution of periodontal inflammation [24]. We compared the levels of all

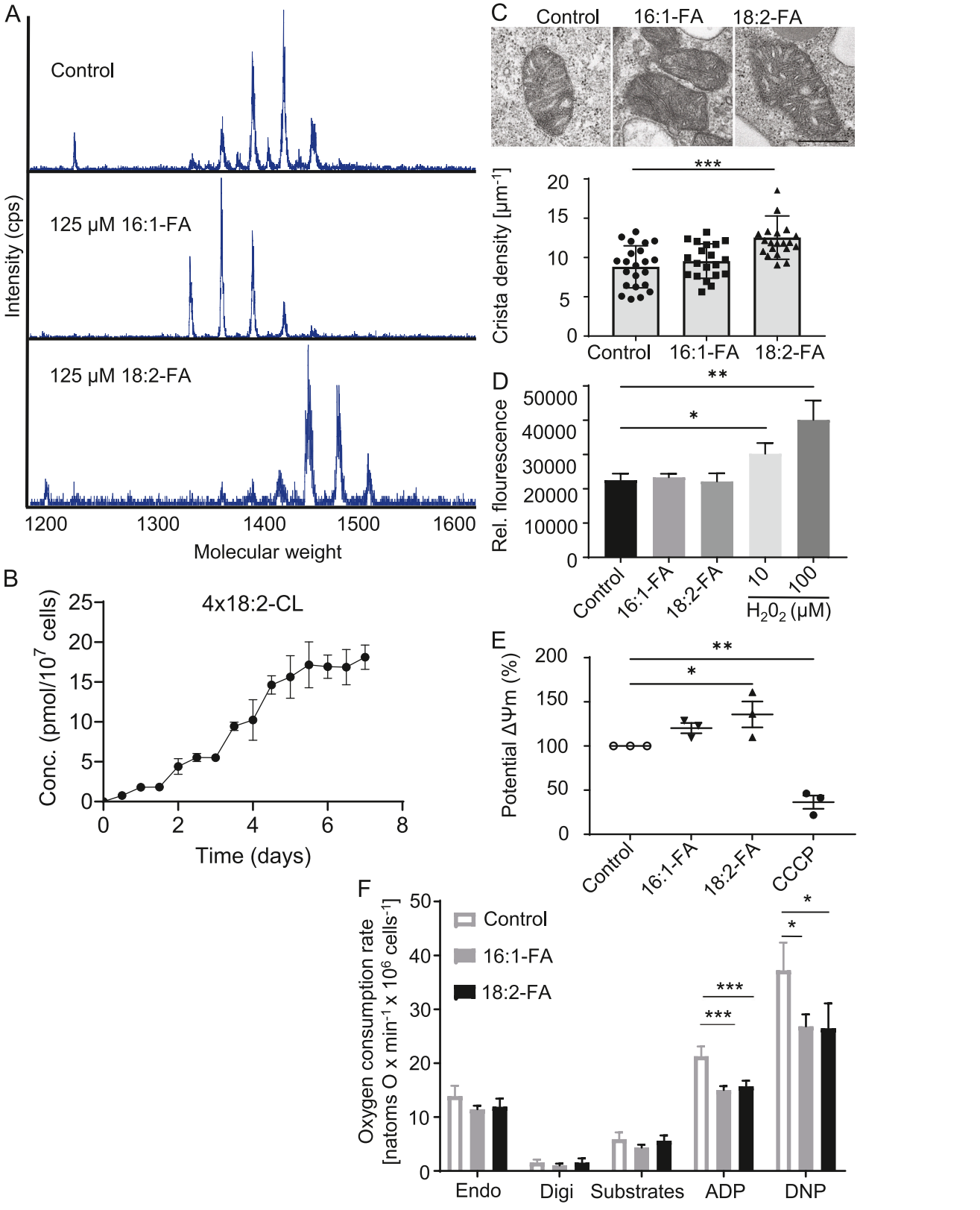

(caption on next page)

Fig. 4. Cultivated J774A.1 mouse macrophages supplemented with 16:1-FA or 18:2-FA as indicated. (A) Representative illustration of precursor ion scans of the fragment m/z 153 of one out of three independent experiments. (B) Amount of 4 × 18:2-CL in J774A.1 cell samples supplemented with 18:2-FA for 7 days. Data are shown as mean ± SD of two independent experiments. (C) Representative electron microscopy images of mitochondria in J774A.1 mouse macrophages. For quantification, 20–22 mitochondria were randomly selected from at least ten cells per condition. Data are shown as mean ± SD, $n = 20–22$, ***$p < 0.001$, scale bar: 500 nm. (D) Reactive oxygen species (ROS) assay. Hydrogen peroxide (H_2O_2) was used as positive control. Data are shown as mean ± SD of three independent experiments. Statistical analysis was performed using the one-way ANOVA test followed by Tukey's multiple comparison test, with *$p < 0.05$, **$p < 0.01$. (E) Mitochondrial membrane potential determined by the fluorescent dye JC-1. Shown are relative values compared to controls, which were set to 100 %. A positive control was generated by using the uncoupler carbonyl cyanide *m*-chlorophenyl hydrazine (CCCP). Data are shown as mean ± SD of three independent experiments. Statistical analysis was performed using the one-way ANOVA test followed by Tukey's multiple comparison test, with *$p < 0.05$, **$p < 0.01$. (F) Oxygen consumption rates of J774 control and treated (16:1-FA, 18:2-FA) cells under different conditions. Data are shown as mean + SEM of $n = 4$ individual experiments. Endo – oxygen consumption of intact cells, Digi – digitonin for cell permeabilisation, Substrates – complex I linked: pyruvate 5 mM + glutamate 5 mM + 2 mM malate in absence of ADP for non-phosphorylating respiration, ADP - 2 mM for inducing maximal respiration, DNP - 2,4-dinitrophenol for inducing uncoupled respiration, one-way ANOVA and Tukey's multiple comparison test were performed with *$p < 0.05$, **$p < 0.01$.

analyzed CL in the three groups using principal component (PC) analysis (Fig. 5C). The results showed an overlap between the 16:0-FA supplemented group and the control group, but distinct differences in the 18:1-FA supplemented mice. This suggests that supplementation with 16:0-FA did not alter the CL profile, consistent with the general observation that saturated FAs are rarely found in CL. In contrast, the CL profile of the 18:1-FA supplemented mice differed significantly, which was in line with the common presence of 18:1-FA residues in tissues lacking 18:2-FA. We further specified the changes in the CL profile using LC-MS/MS in the MRM mode. The 3 × 18:2/1 × 16:1-CL variant was less expressed following 18:1-FA supplementation (Fig. 5D). Conversely, the levels of CL variants with a high content of 18:1-FA residues were significantly increased (Fig. 5E,F). Supplementation with 16:0-FA did not affect the CL profile (Fig. 5G-I).

4. Discussion

In this study, we examined the distribution of CLs across various tissues. The quantitative differences between the peripheral organs were likely caused by different cellular amounts of mitochondria. There is evidence that the level of CL is directly linked to the number of mitochondria [32] with both tissues, heart and liver, being mitochondria-rich, though heart muscle has an especially high mitochondrial content [33]. We found the most notable qualitative differences in the brain, which is a tissue with distinct metabolic properties. Among the FAs analyzed, only 18:2-FA exhibited a significant decrease, possibly due to the blood brain barrier isolating the brain tissue from systemic circulation. Although essential linoleic acid is taken up by the brain from circulation, palmitic, stearic and oleic acids are not. They are formed locally by *de novo* synthesis, indicating a unique role of FA transportation and synthesis in the brain [34]. Our observations in cell culture also revealed significant deviations in CL composition, associated with a lower level of 18:2-FA in FBS compared to human serum. Markedly, the CL profiles of J774A.1 cells, representing a classic immortalized cell line, and VSMCs, representing primary non-immortalized cells, did not differ significantly from each other. This indicates that the cell type or degree of immortalization is not a major determinant of the cardiolipin profile under cell culture conditions, but rather the consequence of FA availability provided through media supplements such as FBS. Previous research suggested that the ratio of 18:2-FA to 18:1-FA as part of other phospholipids is critical in determining the CL profile. Higher levels of 18:2-FA promote their incorporation into CL, whereas increased 18:1-FA levels favor the formation of alternative CL variants [35]. Our findings are consistent with these observations on the level of FAs, directly reflected in the FA profiles and CL variants. The unique FA profile of FBS and its impact on CL expression emphasize the need to carefully evaluate the FA composition of cell culture media. To more accurately model peripheral mitochondrial phenotypes, using human serum instead of FBS or maintaining a stable level of 18:2-FA, may prove beneficial.

An interesting aspect of our study is that we identified aging as a factor that influences CL composition across all examined tissues. Other studies have reported a decline in the total CL content with age in different compartments, associated with functional impairment [36,37]. Our findings also demonstrate a significant alteration in the qualitative composition of CLs, characterized by a marked decrease in CL with 18:2-FA residues. This shift is accompanied by a significant increase in CLs containing both, shorter (C16) and longer (C20 or C22) FA side chains. This fits with the observations in other studies, *e.g.*, in heart tissue, where a decrease in the 4 × 18:2-CL and an increase in longer unsaturated FA residues have been demonstrated in absolute values [38]. Similar alterations may have a link to pathological conditions in this organ [39,40]. The decrease in 18:2-FA residues could impair mitochondrial function, with 4 × 18:2-CL potentially playing an important role in stimulating essential processes such as mitochondrial respiration [22,41]. On the other hand, the higher proportion of other FAs, such as 22:6-FA, could negatively impact the activity of key mitochondrial enzymes and processes [42].

Our cell culture experiments demonstrated the significant influence of altered FA supply on the CL profile for cells in culture. By maintaining high and constant FA concentrations with two supplementations per day, we induced maximal changes in the CL profile. However, even higher FA concentrations resulted in reduced cell viability. Transmission electron microscopy revealed no significant differences in mitochondrial structure between cells treated with 16:1-FA and the control group, which is consistent with the already high proportion of 16:1-FA in the standard CL profile of cell cultures. In contrast, the addition of 18:2-FA exerted an increase in mitochondrial cristae, which may enhance the functional capacity of the respiratory chain. The observed increase in mitochondrial membrane potential following 18:2-FA supplementation is indicative for a major influence of 18:2-FA containing CL on mitochondrial activity, likely contributing to improved cellular health [31,43]. Interestingly, there was no difference in ROS production between the control group and cells treated with FAs, despite an increase in the MMP. Mitochondria are considered as the main source of ROS in cells, and there is a strong positive correlation of the MMP and ROS production [44]. The absence of a positive correlation suggests that 18:2-containing CL may also play a role in regulating ROS balance, *e.g.*, increasing cells' antioxidative capacity or preventing excessive ROS production and cell damage.

The mouse model experiments validated our cell culture findings and provided further insights into the dynamics of CL profile changes *in vivo*. Here, we focused on liver samples, but it would be useful to extend these analyses to other organ systems. The liver's role as a storage organ for lipids and fatty acids, including triglycerides, implies dynamic storage and release processes, and these dynamics might be even more pronounced in other organs. Nevertheless, our results showed a noticeable increase in the supplemented fatty acid in comparison to the control group. Future studies should consider measuring serum FA levels to assess systemic circulation. Remarkably, supplementation with 16:0-FA did not alter the CL profile, suggesting that saturated fatty acids are not preferential substrates for CL synthesis and remodeling under physiological conditions. However, increased 16:0-FA residues have been reported in pathological conditions such as Barth syndrome [12].

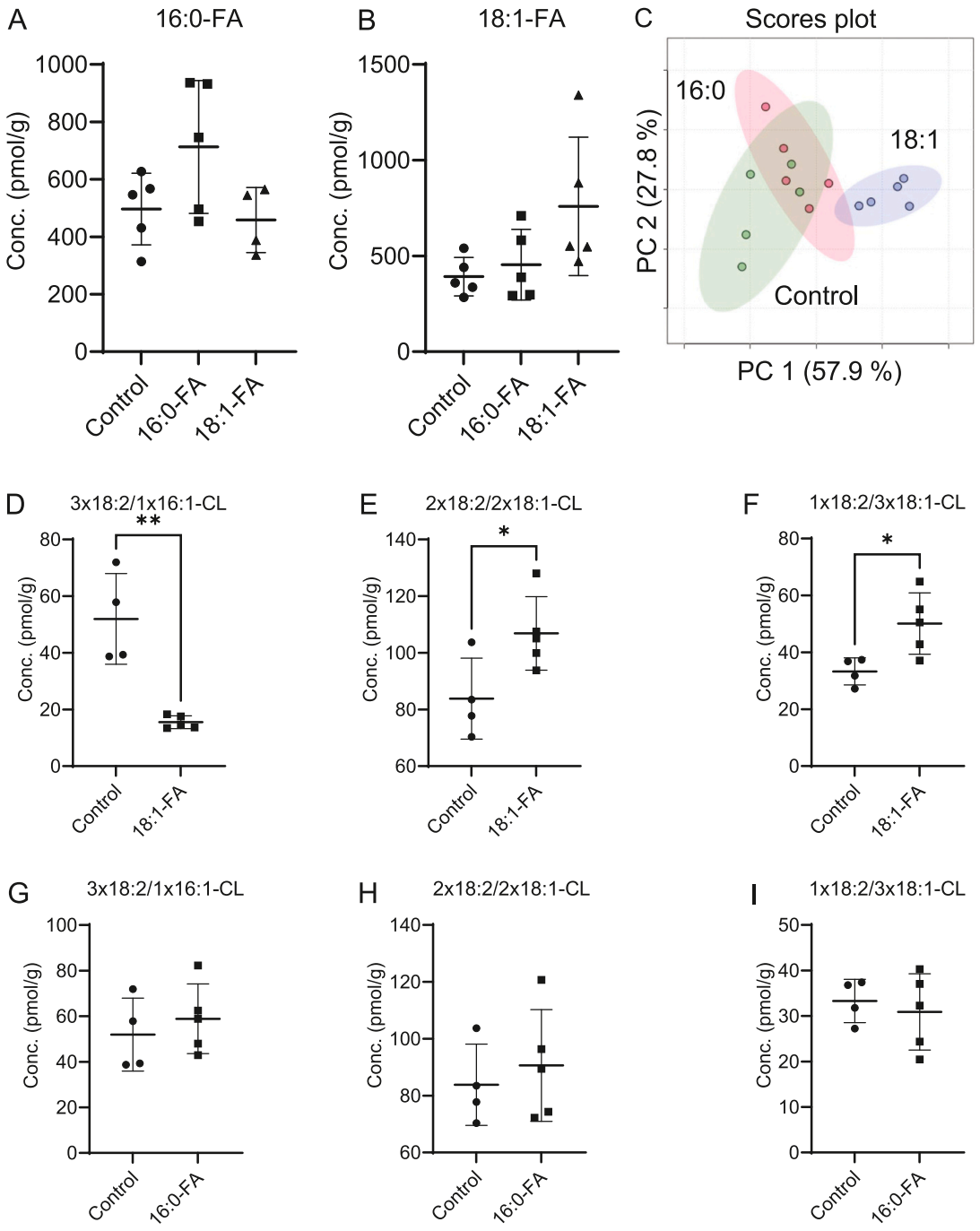

Fig. 5. FA levels and CL profiles in liver samples of FA-supplemented mice as indicated. (A-B) Concentration of 16:0-FA and 18:1-FA in liver samples from mice on a 16:0-FA or 18:1-FA diet compared with control mice receiving normal chow. (C) Principal component (PC) analysis performed with the web-based platform MetaboAnalyst [47]. (D-F) Comparison of CL concentrations in liver samples from mice on a 18:1-FA diet compared with control mice receiving normal chow. (G-I) Comparison of respective CL concentrations in liver samples from mice on a 16:0-FA diet compared with control mice receiving normal chow. Data are shown as mean ± SD of 4–5 individual mice per group. Statistical analysis was performed for two groups using two-sample Student's t-test and for multiple groups using the one-way ANOVA test followed by Tukey's multiple comparison test, with *$p < 0.05$, **$p < 0.01$.

Supplementation with 18:1-FA, an unsaturated FA often present in CL, resulted in a moderately significant increase in CL variants containing high amounts of 18:1-FA and 18:2-FA, while the amount of 3 × 18:2/1 × 16:1-CL decreased significantly, indicating a potential replacement of 16:1-FA residues by 18:1-FA. The addition of other fatty acids, *e.g.*, long-chain unsaturated fatty acids, could further influence the CL profile and mitochondrial function, as previously demonstrated [42]. This could have implications for modulating the activity of the respiratory chain. Dietary manipulation of FA composition presents a potential strategy to alter the CL profile with functional impact on mitochondria. Further studies are required to determine the applicability to humans. Such an approach may also offer therapeutic potential for reversing age-related mitochondrial dysfunction, with 18:2-FA being a particularly promising candidate, specifically with its increasing effects on the tetralinoleoyl-CL and its effect on the mitochondrial activity [41]. Future investigations are necessary to validate these findings.

Finally, changes in CL acyl chain composition can have profound implications for mitochondrial function. CL is indispensable for

maintaining cristae architecture and stabilizing respiratory chain supercomplexes, thereby enhancing oxidative phosphorylation, *i.e.*, ATP synthesis [45]. It also anchors key proteins such as ATP synthase and the ADP/ATP carrier, directly affecting energy transduction. Moreover, remodeling of cardiolipin has been linked to elevated mitochondrial ROS production and sensitization towards apoptosis *via* CL peroxidation and cytochrome *c* release [8]. Importantly, there is increasing evidence for CL being involved in mitochondrial dynamics, quality control mechanisms like mitophagy and membrane contact site signaling [46]. Our data provide a biochemical basis for future investigations into how altered cardiolipin composition may affect mitochondrial structure and function.

Taken together, with the comparison of tissues from different origin and age, we highlight the dynamic changes of CL composition regarding its important role for the mitochondrial membrane architecture and the activity status. We identified the FA composition as a crucial factor to actively induce alterations in the CL profile. This opens up interesting treatment strategies for age-dependent improvement of mitochondrial function.

CRediT authorship contribution statement

Philipp W. Weiß: Writing – review & editing, Writing – original draft, Visualization, Validation, Methodology, Investigation, Funding acquisition, Formal analysis, Data curation, Conceptualization. **Philip P. Kaltenborn:** Writing – review & editing, Validation, Methodology, Investigation, Formal analysis. **Christiane Frahm:** Writing – review & editing, Resources. **Ulrike Schulze-Späte:** Writing – review & editing, Resources. **Estelle Heyne:** Formal analysis, Investigation, Methodology, Writing – review & editing. **Marten Szibor:** Writing – review & editing. **Sandor Nietzsche:** Writing – review & editing, Methodology. **Ralf A. Claus:** Writing – review & editing, Writing – original draft, Project administration. **Markus H. Gräler:** Writing – review & editing, Writing – original draft, Supervision, Resources, Project administration, Funding acquisition, Conceptualization.

Declaration of competing interest

The authors declare that the research was conducted in the absence of any commercial or financial relationships that could be construed as a potential conflict of interest.

Acknowledgments

The study was supported by the CSCC (Center for Sepsis Control and Care) to MHG. We also gratefully acknowledge support by JSAM (Jena School for Aging Medicine) to PWW, by the Carl Zeiss Foundation IMPULS programme (project number: P2019-01-006) to *CF*, by the German Federal Ministry of Education and Research (BMBF, 01EC1901B, Project 2) to USS, and by the Open Access Publication Fund of the Thueringer Universitäts- und Landesbibliothek (ThULB) Jena. We express our gratitude to Mareike Schilder and Faiza Nazar for their valuable support and contributions to this study. We (PWW & PPK) also appreciate the insightful feedback from our peers, which greatly improved the quality of this work.

Data availability

All materials and data generated in this study are available upon request. Interested researchers may contact the corresponding author (MHG).

References

[1] Y. Tamura, S. Kawano, T. Endo, Lipid homeostasis in mitochondria, Biol. Chem. 401 (2020) 821–833.
[2] M. Ren, C.K. Phoon, M. Schlame, Metabolism and function of mitochondrial cardiolipin, Prog. Lipid Res. 55 (2014) 1–16.
[3] A.K. Kondadi, R. Anand, A.S. Reichert, Cristae membrane dynamics - a paradigm change, Trends Cell Biol. 30 (2020) 923–936.
[4] Y. Lee, C. Willers, E.R. Kunji, P.G. Crichton, Uncoupling protein 1 binds one nucleotide per monomer and is stabilized by tightly bound cardiolipin, Proc. Natl. Acad. Sci. U. S. A. 112 (2015) 6973–6978.
[5] M. Zhang, E. Mileykovskaya, W. Dowhan, Gluing the respiratory chain together. Cardiolipin is required for supercomplex formation in the inner mitochondrial membrane, J. Biol. Chem. 277 (2002) 43553–43556.
[6] M. Ott, B. Zhivotovsky, S. Orrenius, Role of cardiolipin in cytochrome c release from mitochondria, Cell Death Differ. 14 (2007) 1243–1247.
[7] G. Petrosillo, G. Casanova, M. Matera, F.M. Ruggiero, G. Paradies, Interaction of peroxidized cardiolipin with rat-heart mitochondrial membranes: induction of permeability transition and cytochrome c release, FEBS Lett. 580 (2006) 6311–6316.
[8] J. Dudek, Role of cardiolipin in mitochondrial signaling pathways, Front. Cell Dev. Biol. 5 (2017) 90.
[9] Y. Tamura, Y. Harada, S. Nishikawa, K. Yamano, M. Kamiya, T. Shiota, T. Kuroda, O. Kuge, H. Sesaki, K. Imai, K. Tomii, T. Endo, Tam41 is a CDP-diacylglycerol synthase required for cardiolipin biosynthesis in mitochondria, Cell Metab. 17 (2013) 709–718.
[10] J. Zhang, Z. Guan, A.N. Murphy, S.E. Wiley, G.A. Perkins, C.A. Worby, J.L. Engel, P. Heacock, O.K. Nguyen, J.H. Wang, C.R. Raetz, W. Dowhan, J.E. Dixon, Mitochondrial phosphatase PTPMT1 is essential for cardiolipin biosynthesis, Cell Metab. 13 (2011) 690–700.
[11] D. Chen, X.Y. Zhang, Y. Shi, Identification and functional characterization of hCLS1, a human cardiolipin synthase localized in mitochondria, Biochem. J. 398 (2006) 169–176.
[12] Y. Xu, J.J. Sutachan, H. Plesken, R.I. Kelley, M. Schlame, Characterization of lymphoblast mitochondria from patients with Barth syndrome, Lab. Invest. 85 (2005) 823–830.
[13] P.G. Barth, R.J. Wanders, P. Vreken, X-linked cardioskeletal myopathy and neutropenia (Barth syndrome)-MIM 302060, J. Pediatr. 135 (1999) 273–276.
[14] M. Schlame, Cardiolipin remodeling and the function of tafazzin, Biochim. Biophys. Acta 1831 (2013) 582–588.
[15] C. Lopez-Otin, M.A. Blasco, L. Partridge, M. Serrano, G. Kroemer, The hallmarks of aging, Cell 153 (2013) 1194–1217.
[16] A. Navarro, A. Boveris, The mitochondrial energy transduction system and the aging process, Am. J. Physiol. Cell Physiol. 292 (2007) C670–C686.
[17] G. Lenaz, C. Bovina, C. Castelluccio, R. Fato, G. Formiggini, M.L. Genova, M. Marchetti, M.M. Pich, F. Pallotti, G. Parenti Castelli, G. Biagini, Mitochondrial complex I defects in aging, Mol. Cell. Biochem. 174 (1997) 329–333.
[18] D. Hornburg, S. Wu, M. Moqri, X. Zhou, K. Contrepois, N. Bararpour, G.M. Traber, B. Su, A.A. Metwally, M. Avina, W. Zhou, J.M. Ubellacker, T. Mishra, S. M. Schussler-Fiorenza Rose, P.B. Kavathas, K.J. Williams, M.P. Snyder, Dynamic lipidome alterations associated with human health, disease and ageing, Nat. Metab. 5 (2023) 1578–1594.
[19] G. Xu, X. Liu, Y. Shu, J.A. Pillai, Y. Xu, A rapid and sensitive LC-MS/MS method for quantitative analysis of cardiolipin (18:2)(4) in human leukocytes and mouse skeletal muscles, J. Pharm. Biomed. Anal. 158 (2018) 386–394.
[20] M. Schlame, D. Acehan, B. Berno, Y. Xu, S. Valvo, M. Ren, D.L. Stokes, R.M. Epand, The physical state of lipid substrates provides transacylation specificity for tafazzin, Nat. Chem. Biol. 8 (2012) 862–869.
[21] G. Oemer, K. Lackner, K. Muigg, G. Krumschnabel, K. Watschinger, S. Sailer, H. Lindner, E. Gnaiger, S.B. Wortmann, E.R. Werner, J. Zschocke, M.A. Keller, Molecular structural diversity of mitochondrial cardiolipins, Proc. Natl. Acad. Sci. U. S. A. 115 (2018) 4158–4163.
[22] D.B. Snoke, C.A. Mahler, A. Angelotti, R.M. Cole, G.C. Sparagna, K.K. Baskin, M. A. Belury, Linoleic acid-enriched diet increases mitochondrial tetralinoleoyl cardiolipin, OXPHOS protein levels, and uncoupling in interscapular brown adipose tissue during diet-induced weight gain, Biology (Basel) 12 (2022).
[23] M. Olecka, A. van Bommel, L. Best, M. Haase, S. Foerste, K. Riege, T. Dost, S. Flor, O.W. Witte, S. Franzenburg, M. Groth, B. von Eyss, C. Kaleta, C. Frahm, S. Hoffmann, Nonlinear DNA methylation trajectories in aging male mice, Nat. Commun. 15 (2024) 3074.
[24] A. Doding, S. Zimmermann, A. Maghames, M. Reimann, J. Symmank, M. Thurmer, M.H. Graler, M. Wolf, C. Jacobs, A. Koeberle, B. Sigusch, U. Schulze-Spate, Immunometabolic capacities of nutritional fatty acids in regulation of inflammatory bone cell interaction and systemic impact of periodontal infection, Front. Immunol. 14 (2023) 1213026.
[25] L. Giordano, M.K. Aneja, N. Sommer, N. Alebrahimdehkordi, A. Seraji, N. Weissmann, C. Rudolph, C. Plank, H.T. Jacobs, M. Szibor, Alternative oxidase encoded by sequence-optimized and chemically-modified RNA transfected into mammalian cells is catalytically active, Gene Ther. 29 (2022) 655–664.
[26] E. Heyne, S. Zeeb, C. Junker, A. Petzinna, A. Schrepper, T. Doenst, L.G. Koch, S. L. Britton, M. Schwarzer, Exercise training differentially affects skeletal muscle mitochondria in rats with inherited high or low exercise capacity, Cells 13 (2024).
[27] G. Oemer, M.L. Edenhofer, Y. Wohlfarter, K. Lackner, G. Leman, J. Koch, L.H. D. Cardoso, H.H. Lindner, E. Gnaiger, S. Dubrac, J. Zschocke, M.A. Keller, Fatty acyl availability modulates cardiolipin composition and alters mitochondrial function in HeLa cells, J. Lipid Res. 62 (2021) 100111.
[28] H.C. Ting, Y.J. Chao, Y.H. Hsu, Polyunsaturated fatty acids incorporation into cardiolipin in H9c2 cardiac myoblast, J. Nutr. Biochem. 26 (2015) 769–775.
[29] T.G. Frey, C.A. Mannella, The internal structure of mitochondria, Trends Biochem. Sci. 25 (2000) 319–324.

[30] K. Brieger, S. Schiavone, F.J. Miller Jr., K.H. Krause, Reactive oxygen species: from health to disease, Swiss Med. Wkly. 142 (2012) w13659.
[31] L.B. Chen, Mitochondrial membrane potential in living cells, Annu. Rev. Cell Biol. 4 (1988) 155–181.
[32] S. Larsen, J. Nielsen, C.N. Hansen, L.B. Nielsen, F. Wibrand, N. Stride, H. D. Schroder, R. Boushel, J.W. Helge, F. Dela, M. Hey-Mogensen, Biomarkers of mitochondrial content in skeletal muscle of healthy young human subjects, J. Physiol. 590 (2012) 3349–3360.
[33] J. Piquereau, F. Caffin, M. Novotova, C. Lemaire, V. Veksler, A. Garnier, R. Ventura-Clapier, F. Joubert, Mitochondrial dynamics in the adult cardiomyocytes: which roles for a highly specialized cell? Front. Physiol. 4 (2013) 102.
[34] J. Edmond, T.A. Higa, R.A. Korsak, E.A. Bergner, W.N. Lee, Fatty acid transport and utilization for the developing brain, J. Neurochem. 70 (1998) 1227–1234.
[35] G. Oemer, J. Koch, Y. Wohlfarter, M.T. Alam, K. Lackner, S. Sailer, L. Neumann, H. H. Lindner, K. Watschinger, M. Haltmeier, E.R. Werner, J. Zschocke, M.A. Keller, Phospholipid acyl chain diversity controls the tissue-specific assembly of mitochondrial Cardiolipins, Cell Rep. 30 (2020) 4281–4291 e4284.
[36] Y. Yoo, M. Yeon, W.K. Kim, H.B. Shin, S.M. Lee, M.S. Yoon, H. Ro, Y.K. Seo, Age-dependent loss of Crls1 causes myopathy and skeletal muscle regeneration failure, Exp. Mol. Med. 56 (2024) 922–934.
[37] G. Paradies, F.M. Ruggiero, G. Petrosillo, E. Quagliariello, Age-dependent decline in the cytochrome c oxidase activity in rat heart mitochondria: role of cardiolipin, FEBS Lett. 406 (1997) 136–138.
[38] H.J. Lee, J. Mayette, S.I. Rapoport, R.P. Bazinet, Selective remodeling of cardiolipin fatty acids in the aged rat heart, Lipids Health Dis. 5 (2006) 2.
[39] G.C. Sparagna, A.J. Chicco, R.C. Murphy, M.R. Bristow, C.A. Johnson, M.L. Rees, M.L. Maxey, S.A. McCune, R.L. Moore, Loss of cardiac tetralinoleoyl cardiolipin in human and experimental heart failure, J. Lipid Res. 48 (2007) 1559–1570.
[40] C.M. Mulligan, C.H. Le, A.B. deMooy, C.B. Nelson, A.J. Chicco, Inhibition of delta-6 desaturase reverses cardiolipin remodeling and prevents contractile dysfunction in the aged mouse heart without altering mitochondrial respiratory function, J. Gerontol. A Biol. Sci. Med. Sci. 69 (2014) 799–809.
[41] D.B.S. Connor A. Mahler, Rachel M. Cole, Austin Angelotti, K.K.B. Genevieve C. Sparagna, Ai Ni, Martha A. Belury, Consuming a linoleate-rich diet increases concentrations of tetralinoleoyl cardiolipin in mouse liver and alters hepatic mitochondrial respiration, The Journal of Nutrition 154 (2024) 856–865.
[42] E.M. Sullivan, E.R. Pennington, G.C. Sparagna, M.J. Torres, P.D. Neufer, M. Harris, J. Washington, E.J. Anderson, T.N. Zeczycki, D.A. Brown, S.R. Shaikh, Docosahexaenoic acid lowers cardiac mitochondrial enzyme activity by replacing linoleic acid in the phospholipidome, J. Biol. Chem. 293 (2018) 466–483.
[43] S.R. Pieczenik, J. Neustadt, Mitochondrial dysfunction and molecular pathways of disease, Exp. Mol. Pathol. 83 (2007) 84–92.
[44] J.F. Turrens, Mitochondrial formation of reactive oxygen species, J. Physiol. 552 (2003) 335–344.
[45] Z. Jiang, T. Shen, H. Huynh, X. Fang, Z. Han, K. Ouyang, Cardiolipin regulates mitochondrial ultrastructure and function in mammalian cells, Genes (Basel) 13 (2022).
[46] K.J. Emaus, G.M. Fogo, J.M. Wider, T.H. Sanderson, The role of cardiolipin in mitochondrial dynamics and quality control in neuronal ischemia/reperfusion injury, Cell Death Dis. 16 (2025) 494.
[47] J. Xia, N. Psychogios, N. Young, D.S. Wishart, MetaboAnalyst: a web server for metabolomic data analysis and interpretation, Nucleic Acids Res. 37 (2009) W652–W660.